Hindawi
International Journal of RF and Microwave Computer-Aided Engineering
Volume 2024, Article ID 6300533, 11 pages
https://doi.org/10.1155/2024/6300533

Research Article

A Collaborative Control Method of Transmission Amplitude and Phase for Transmitarray Antenna Design

Dawei Ding,[1,2] **Junfeng Chen**,[1] **Guang Li**,[1] **and Hailin Hong**[2]

[1]*School of Electronic and Information Engineering, Anhui University, Hefei, China*
[2]*Information Materials and Intelligent Sensing Laboratory of Anhui Province, Anhui University, Hefei, China*

Correspondence should be addressed to Dawei Ding; 19119@ahu.edu.cn

Received 8 January 2024; Revised 16 February 2024; Accepted 5 March 2024; Published 25 March 2024

Academic Editor: Piotr Gas

In this paper, a collaborative control method of transmission amplitude and phase for transmitarray antenna (TA) design is proposed. In this proposed method, one of the most popular hypersurface fitting models, Gaussian stochastic process (GP) model, is utilized to construct an accurate surrogate model. Following this implementation, a mapping relationship between structural parameters of TA unit cell and its transmission amplitude and phase is established. The most advantage of this method is its applicability for general TA designs because it is much difficult to control the amplitude and phase of unit cell independently through adjusting separate structural parameters. To verify the high efficiency of the proposed method, three TA antennas with different scanning angles are designed to obtain high sidelobe suppression level. Measured results show that the proposed collaborative control method of amplitude and phase is much promising for high sidelobe suppression level in TA designs.

1. Introduction

A transmitarray (TA) antenna typically consists of a focal source and an array of TA unit cells, where each unit cell provides a certain transmission phase shift to compensate for the different path lengths from the focal source [1–3]. TA antenna achieves desired radiation characteristics through converting the incident wave from the focal source into an expected outgoing wave. In the past decades, TA antennas have received more and more attention because of its advantages derived from both lens antennas and microstrip arrays, such as high gain, flexible radiation performances, low profile, light weight, simple processing technology, cheap fabrication cost, and no insertion loss caused by the feeding network of phased array [1]. Unfortunately, like microstrip phased arrays, TA designs still suffer from some urgent problems, such as limited bandwidth, low sidelobe suppression level (SLL), and low aperture efficiency.

In most TA designs, a unit cell with transmission phase range of more than 300° and transmission magnitude as high as possible is usually necessary to obtain enough design freedom and low insertion loss [2, 3]. In these designs, only phase distribution had been assigned to synthesize the required radiation performances, and SLL of less than 12 dB at boresight direction had been obtained, which could not satisfy requirements in many applications, such as radar systems and mobile communication systems. In order to improve SLL and increase degree of freedom, both transmission magnitude and phase had been optimized in [4–7]. In these designs, it is expected to independently control transmission magnitude and phase through adjusting different structural parameters, respectively. Meanwhile, transmission magnitude and phase should be "decoupled" [7]. Unfortunately, it is hard to absolutely independently control (i.e. "decouple") magnitude and phase. That is, phase could be adjusted through changing one structural parameter, while magnitude might also be varied, and vice versa. In addition, in these designs, large variation regions of transmission magnitude and phase are determined as [0, 1] and [0°, 360°], which extremely increases the design difficulty of TA

unit cell. Therefore, a collaborative control method of transmission magnitude and phase of unit cell is in much demand for TA designs.

For the aforementioned problem, a method for accurately predicting the transmission magnitude and phase of a given structural parameters of TA unit cell could provide an efficient solution, which is called surrogate model. Surrogate model, also known as response surface model, is a simplified mathematical representation for approximating a complex real-life system or process [8–12]. The main advantage of surrogate model is its rapid and reliable predictions for the transmission magnitude and phase of TA unit cell (output variables) according to its structural parameters (input variables) without extensive and computationally expensive full-wave electromagnetic (EM) simulations. Data-driven surrogate models are widely used in microwave device designs to optimize realized gain [10], scattering parameters [13, 14], reflection phase characteristics in reflectarrays [15], characteristic impedance [16], and resonant frequency of antenna [17]. There are many kinds of surrogate models, such as regression models [18], neural networks [19, 20], support vector machines [21], and Gaussian process models [22–24]. Gaussian stochastic process (GP) model has become one of the most efficient surrogate models due to its few hyperparameters and high accuracy [23, 24]. In order to obtain the optimal structural parameters according to the built GP models, multiobjective evolutionary algorithm based on decomposition (MOEA/D) is employed due to its global and fast searching abilities for solving the discontinuous, nondifferential, multimodal, and noisy functions [25].

Following this idea, a collaborative control method of transmission magnitude and phase of TA unit cell is proposed in this paper. Compared with the existing control methods in [4–7], the difference is that both transmission magnitude and phase are optimized simultaneously in this collaborative control technique, rather than independently controlling them. The major advantage of this proposed method is the applicability for general TA unit cell without decoupling amplitude and phase. The major contributions of this paper are listed as follows. (1) Compared with the existing TA design procedures, a new and simple strategy for TA designs is proposed, which is an inverse design process. (2) Compared with the existing TA design methods, this proposed method is more suitable for general TA unit cells because it is not necessary to absolutely decouple amplitude and phase which is difficult for most TA unit cell designs. (3) The proposed method releases the design pressure of the unit cell with transmission magnitude varying from 0 to 1 and phase varying from 0° to 360° which is much difficult in practice. The novelties of this work are summarized as follows. (1) A complete and rapid synthesis procedure of TA antenna is proposed by using accurate GP-based surrogate models, where two GP models are employed to construct the mapping relationship from the structural parameters of TA unit cell to its transmission amplitude and phase, respectively, rather than from amplitude and phase to structural parameters. (2) This synthesis procedure could collaboratively control the transmission magnitude and phase of TA, rather than independently controlling them. To the best of our knowledge, it is the first work to propose a collaborative control method of transmission magnitude and phase of TA.

This paper is organized as follows. Section 2 lists the working principle of the proposed collaborative control method of transmission magnitude and phase of TA unit cell in detail, along with the whole design procedure and some design guidelines. Section 3 gives some design examples by using the proposed method. Section 4 concludes this work.

2. Working Principle of Collaborative Control of Transmission Magnitude and Phase

In this section, basic working principle of this proposed collaborative control method of transmission magnitude and phase is given. In this method, GP-based surrogate model is built by using Gaussian stochastic process model [23], and MOEA/D serves as an optimizer [25]. The organization relationship of this section is illustrated in Figure 1 for clear description.

2.1. Gaussian Stochastic Process Model. In a TA design, the numerical relationship between the structural parameters of TA unit cell and its transmission magnitude and phase could be formulated as follows.

$$(y_1, y_2) = f(x_1, x_2, \cdots, x_n), \tag{1}$$

where y_1 and y_2 represent transmission magnitude and phase, $x_i (i = 1, 2, \cdots, n)$ denotes structural parameter, n is the number of structural parameters, and f is a mapping from n -dimensional space to two-dimensional space.

In order to build an accurate surrogate model to replace the complicated and unknown mapping shown in Equation (1), Gaussian stochastic process model is employed, which is based on the following assumption. For any $x = (x_1, x_2, \cdots, x_n)$, $f(x)$ is a sample of a Gaussian random variable $\mu + \varepsilon(x)$, where $\varepsilon(x)$ is subject to the normal distribution with σ^2 as its variance, i.e., $\varepsilon(x) \sim N(0, \sigma^2)$. Therefore, the prior distribution of $f(x)$ is Gaussian with mean μ and variance σ^2, that is, $f(x) \sim N(\mu, \sigma^2)$.

Given K sample points, x^j $(j = 1, 2, \cdots, K)$, and their f-function values (y_1^j, y_2^j), both mean μ and variance σ^2 could be estimated as

$$\widehat{\sigma}^2 = \frac{(y - I\widehat{\mu})^T C^{-1} (y - I\widehat{\mu})}{K}, \tag{2}$$

$$\widehat{\sigma}^2 = \frac{(y - I\widehat{\mu})^T C^{-1} (y - I\widehat{\mu})}{K}, \tag{3}$$

where I is a K-dimensional column vector of ones and C is a $K \times K$ matrix in which (i, j)-element is determined as the correlation coefficient

$$\phi^{\mathrm{tr}} = \phi^{\mathrm{in}} + \phi^{\mathrm{TA}}, \tag{4}$$

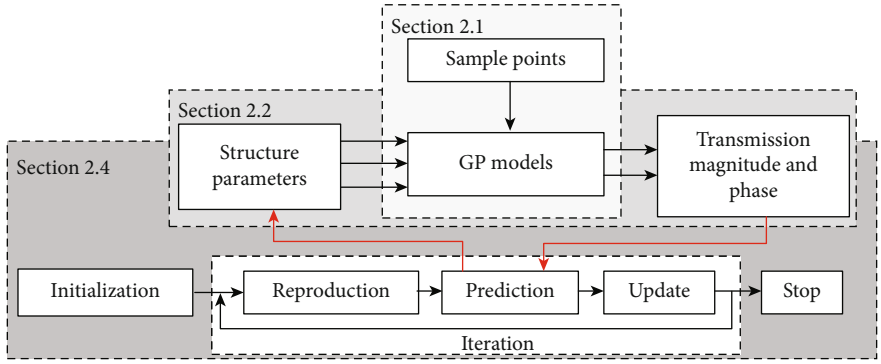

Figure 1: Relationship of this section.

where $\phi^{\mathrm{tr}} = \phi^{\mathrm{in}} + \phi^{\mathrm{TA}}$ is the Euclidean distance between x^i and x^j. Furthermore, the best linear unbiased predictor of $f(x)$ and its mean squared error are calculated as follows.

$$\phi^{\mathrm{tr}} = \phi^{\mathrm{in}} + \phi^{\mathrm{TA}}, \tag{5}$$

$$\phi^{\mathrm{tr}} = \phi^{\mathrm{in}} + \phi^{\mathrm{TA}}, \tag{6}$$

where $\phi^{\mathrm{tr}} = \phi^{\mathrm{in}} + \phi^{\mathrm{TA}}$ is the correlation matrix between sample points and untested point x. Therefore, $\phi^{\mathrm{tr}} = \phi^{\mathrm{in}} + \phi^{\mathrm{TA}}$ can be regarded as a predictive distribution for $f(x)$. Detailed information about GP model could be found in [23, 24]. For easy comprehension, in Figure 2, a GP-based surrogate model is estimated and illustrated by using nineteen samples, where the mean prediction is shown as the solid line and the shaded region denotes twice the standard deviation. It is clearly seen that the predicted values at test points are equal to actual values with zero deviation, and the confidence interval increases with the increased distance between the untested points and sampled points.

In practical applications, in order to train the abovementioned GP-based surrogate model for reflecting the numerical relationship between the structural parameters of TA unit cell and its transmission magnitude and phase, the following detailed steps are suggested. The source code for building GP model could be found in [24].

Step 1 (sampling). Sample K points (i.e., K groups of structure parameters x^j $(j = 1, 2, \cdots, K)$) in design region by using computer experiment methods, such as hypercubic sampling method or random selecting method [24]. Each sample point consists of a vector of all structural parameters of TA unit cell. Then, obtain their f-function values (y_1^j, y_2^j) by using EM simulation software, such as Ansys HFSS or CST Studio Suite.

Step 2 (hyperparameter estimation). Firstly, calculate the sample correlation matrix C according to Eq. (4). Secondly, obtain mean μ and variance σ^2 according to Eqs. (2) and (3). Finally, generate the best linear unbiased predictor of $f(x)$ and its mean squared error according to Eqs. (5) and (6).

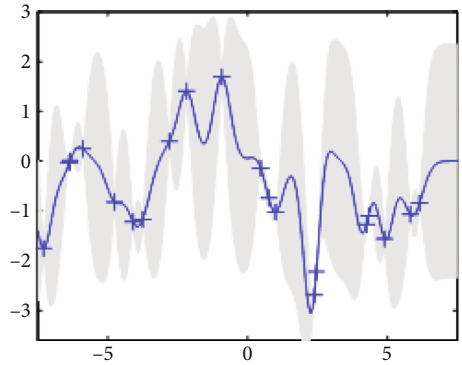

Figure 2: Surrogate model based on Gaussian stochastic process model.

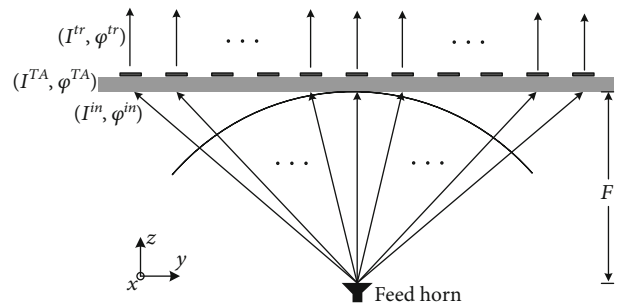

Figure 3: General TA configuration.

Step 3 (model accuracy evaluation). In order to evaluate the accuracy of the trained GP model, either mean squared error (MSE) or mean absolute error (MAE) is used, which is commonly used as performance metric to measure the average squared difference between the predicted and actual values. Detailed calculation process for MSE and MAE could be found in [23, 24]. When MSE or MAE is larger than a preset threshold, more sample points are necessary, and then, repeat Steps 1 and 2. By doing this, the calculated hyperparameters, μ and σ^2, could ensure the trained GP model to be accurate enough [26, 27].

Input: a TA design (i.e., a vector of structure parameters $(x_1, x_2, \cdots x_n)$, n is the product of the scale of TA and the number of structural parameters of unit cell)
Output: its objective function values
Step 1: predict $(\boldsymbol{I}^{\mathbf{TA}}, \boldsymbol{\varphi}^{\mathbf{TA}})$
For each unit cell of this TA design, predict its transmission magnitude and phase by using GP-based surrogate models according to Section 2.1. Then, obtain transmission magnitude and phase distribution of this TA design $(I^{\mathrm{TA}}, \varphi^{\mathrm{TA}})$.
Step 2: calculate $(\boldsymbol{I}^{\mathbf{in}}, \boldsymbol{\varphi}^{\mathbf{in}})$
Given a focal source and its distance to TA aperture F, calculate the amplitude and phase of the incoming wave from the focal source $(I^{\mathrm{in}}, \varphi^{\mathrm{in}})$ according to Eqs. (8) and (9).
Step 3: calculate $(\boldsymbol{I}^{\mathbf{tr}}, \boldsymbol{\varphi}^{\mathbf{tr}})$
Calculate the amplitude and phase generated through TA design according to Eqs. (7) and (10).
Step 4: evaluate objective function values
Firstly, the final transmission magnitude and phase distribution $(I^{\mathrm{tr}}, \varphi^{\mathrm{tr}})$ is used to calculate the overall radiation patterns of this TA antenna according to radiation pattern multiplication principle [29]. Secondly, the objective functions in [30–33] are suggested to extract the optimized radiation characteristics, such as main beam direction, antenna gain, half-power beam width, and SLL.

Algorithm 1: Evaluate objective function values of each TA design.

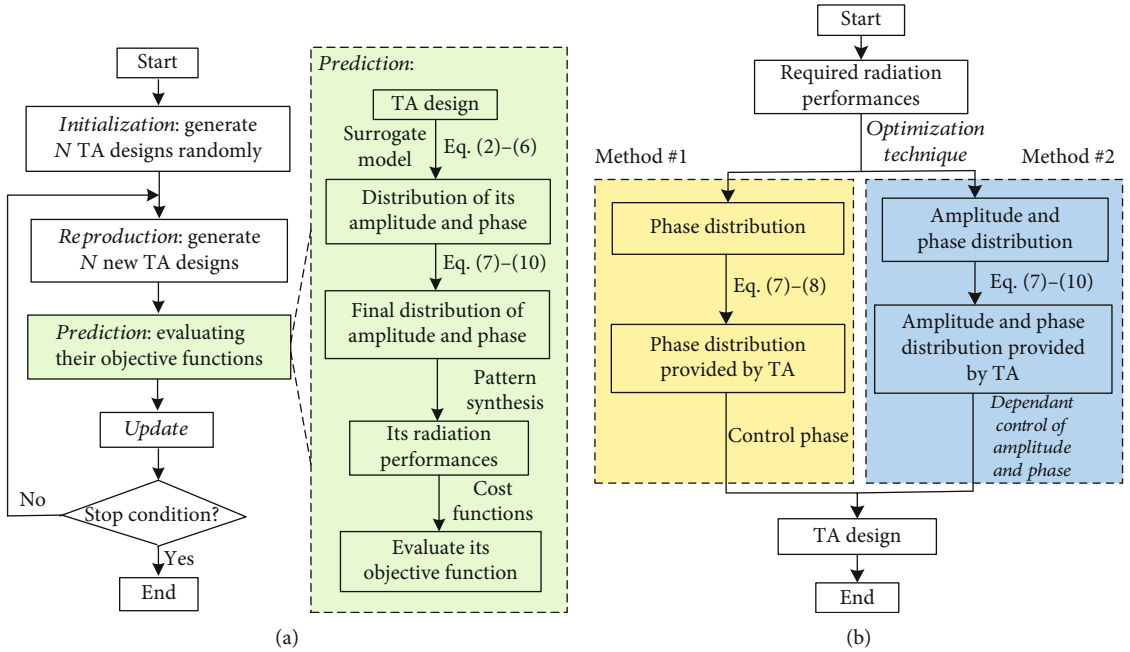

Figure 4: (a) The proposed design procedure: MOEA/D-DE-GP. (b) Two conventional design methods of TA.

Step 4 (predicting). Given a set of structure parameters of TA unit cell, Eq. (5) gives its predicted transmission magnitude/phase. In practical, two GP models are employed to predict transmission amplitude and phase, respectively.

2.2. Collaborative Control of Amplitude and Phase of TA Unit Cell by Using GP Model. Figure 3 illustrates a general TA configuration consisting of many unit cells. The amplitude and phase generated through TA design are denoted as I^{tr} and φ^{tr}. The amplitude and phase provided by a focal source are denoted as I^{in} and φ^{in}. The amplitude attenuation and shifted phase provided by TA unit cell are recognized as I^{TA} and φ^{TA}, respectively. In [4, 28], their relationships are formulated in the following:

$$\phi^{\mathrm{tr}} = \phi^{\mathrm{in}} + \phi^{\mathrm{TA}}, \tag{7}$$

$$\varphi^{\mathrm{in}} = -k_0 \cdot r, \tag{8}$$

$$I^{\mathrm{in}} = \frac{F}{r} \cdot \sqrt{U(\theta)}, \tag{9}$$

$$I^{\mathrm{tr}} = I^{\mathrm{TA}} \cdot I^{\mathrm{in}}, \tag{10}$$

where k_0 is the free-space wavelength, r is the distance between the feed source and unit cell, U is the radiation

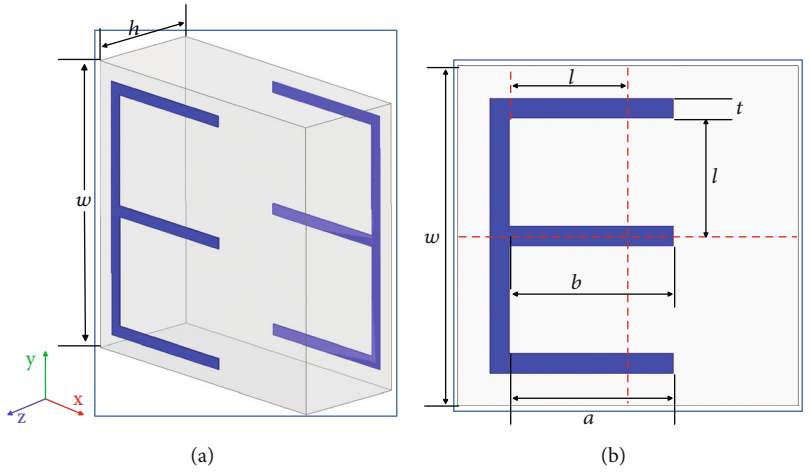

FIGURE 5: The proposed Huygens' unit cell. (a) Overall configuration and (b) top view ($w = 5.2$ mm, $h = 1.5$ mm, $t = 0.2$ mm, $l = 2.1$ mm).

density, and θ is the angle with respect to the main radiation direction.

In order to obtain desired radiation performances, $(I^{\mathrm{TA}}, \varphi^{\mathrm{TA}})$ could be assigned through optimizing the structural parameters of each unit cell, while the built GP model shown in the above subsection is expected to provide accurate surrogate model during optimization process. The following subsection reviews a popular multiobjective optimizer.

In this work, a synthesis procedure of TA antenna based on mathematical processes rather than pure EM simulations or engineering techniques is proposed. The synthesis procedure employs MOEA/D to obtain optimum solutions. In this optimization implementation, it is significantly important to evaluate the objective function values of a given TA design, which is the aim of this subsection Algorithm 1.

2.3. Review of MOEA/D. In 2007, Zhang and Li proposed a new multiobjective optimization framework named as MOEA/D [25]. In the implementation of MOEA/D, multiple design objectives are composed of several subobjectives, where each of them is one aggregation of all design objectives by using weight vector. The weight vector could be recognized as searching direction. Through setting different weight vectors, population could converge to several globally optimal solutions in a single run. It is the major advantage of MOEA/D that it could provide several trading-off candidates for designer's selection. Among many variations of MOEA/D, MOEA/D-DE (MOEA/D combined with differential evolution operators) is much popular. Detailed information about MOEA/D-DE, along with its source code, could be found in [25, 34], and its main flowchart is reviewed in Figure 4(a).

In the past two decades, algorithm performance comparisons have verified its fast searching speed, global optimum, and great algorithm robustness. Moreover, more and more engineering applications in antenna and microwave component have verified the high efficiency of MOEA/D-DE [30–34]. Therefore, it is believed that MOEA/D-DE combined with GP-based surrogate model (MOEA/D-DE-GP)

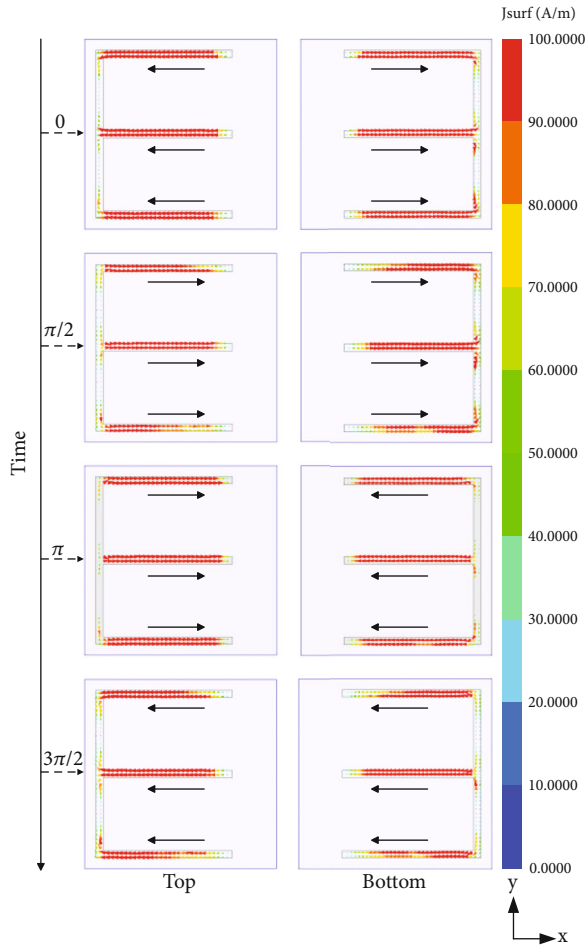

FIGURE 6: Evolution of current distribution at 20 GHz.

could offer a global, parameter-insensitive, fast, and reliable design method for the collaborative control of transmission amplitude and phase of TA design.

2.4. Design Procedure of MOEA/D-DE-GP. In the implementation of MOEA/D-DE-GP, MOEA/D offers a multiobjective

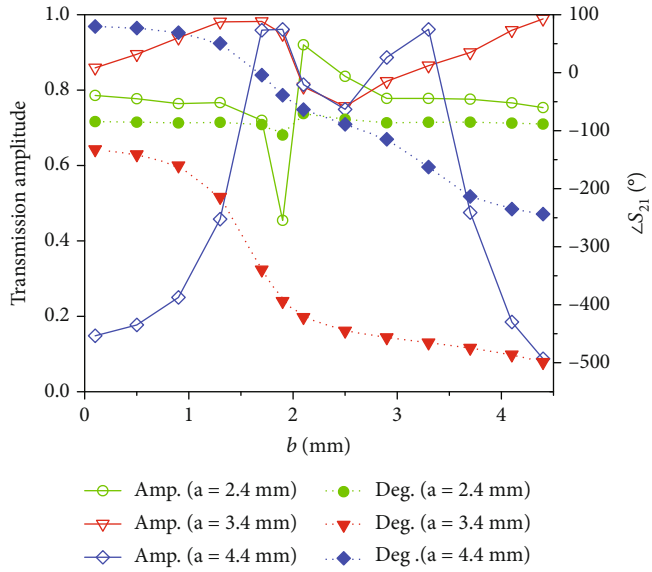

FIGURE 7: Transmission amplitude and phase shift versus different a and b.

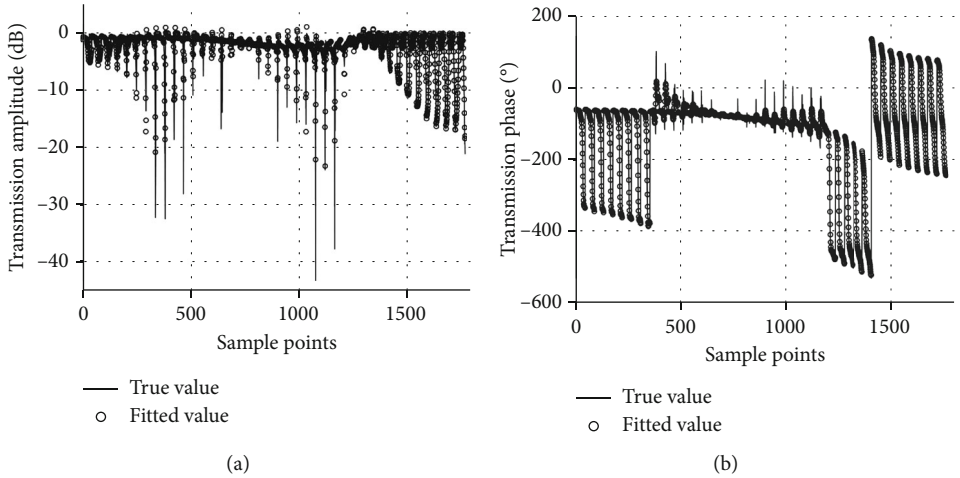

FIGURE 8: Predicted results by using two GP models. (a) Transmission amplitude and (b) transmission phase.

optimization framework, DE provides fast and global evolutionary operators, and GP model serves as an accurate surrogate model to predict the transmission amplitude and phase simultaneously for TA unit cell.

The framework of the proposed method is illustrated in Figure 4(a). For comparison, two general design procedures of TAs are given in Figure 4(b). A step-by-step design procedure of this proposed method for minimization problems is listed as follows.

Step 1 (initialization). Generate N TA designs randomly, and each of them is described to be $(x_1, x_2, \cdots x_n)$, where n is the product of the scale of TA and the number of structural parameters of unit cell. These N TA designs compose an initialized population.

Step 2 (reproduction). For each TA design, its offspring could be generated by using DE operators according to the neighbourhood of this TA design. The detailed procedure of DE operators could be found [25, 34].

Step 3 (prediction). In order to evaluate the fitness value of the newly generated offspring, prediction based on GP-based surrogate model is conducted. Compared with those successful applications in [30–33], it is the major advantage of MOEA/D-DE-GP that objective function could be calculated rapidly through surrogate model, rather than expensive EM simulation. The detailed prediction process is given as follows. Firstly, a surrogate model is built according to Equations (2)–(6). Secondly, $(I^{\mathrm{TA}}, \varphi^{\mathrm{TA}})$ assignment of the offspring $(x_1, x_2, \cdots x_n)$ is predicted according to the built

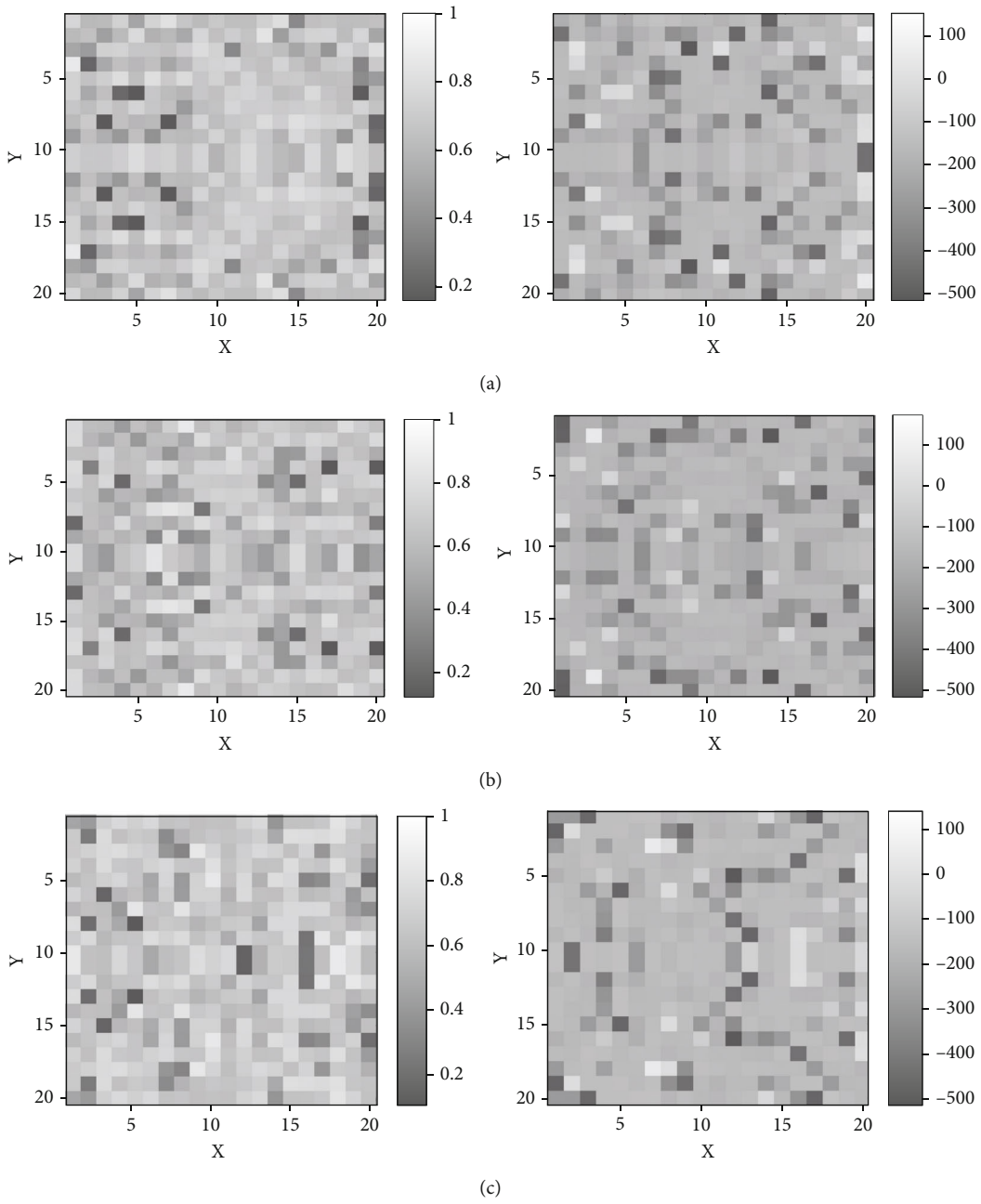

Figure 9: Required amplitude and phase distribution of TA designs. (a) Design I, (b) design II, and (c) design III.

surrogate model. Thirdly, $(I^{\mathrm{tr}}, \varphi^{\mathrm{tr}})$ assignment is derived according to Equations (7)–(10). Then, the radiation performances of this TA design are obtained according to pattern synthesis method. Finally, its objective function is evaluated.

Step 4 (update). When the fitness value of the offspring is smaller than its parents, update it. Otherwise, give up it.

Step 5 (stop condition). When stop condition is satisfied, stop. Otherwise, go to Step 2. Usually, stop condition is set as the maximal iteration times.

It should be noteworthy that the only difference between original MOEA/D-DE and this proposed MOEA/D-DE-GP is Step 3; that is, the objective function values are evaluated by using the predicted amplitude and phase of each unit cell of TA according to the trained GP-based surrogate models, rather than expensive computer simulation and physical experiment. Therefore, it could extremely save computational time and thus provides a highly efficient design procedure, which could be verified in Section 3.3.

In this implementation, it is much important to ensure the accuracy of the trained GP-based surrogate models. Therefore, it is necessary to verify the model accuracy before using this proposed method.

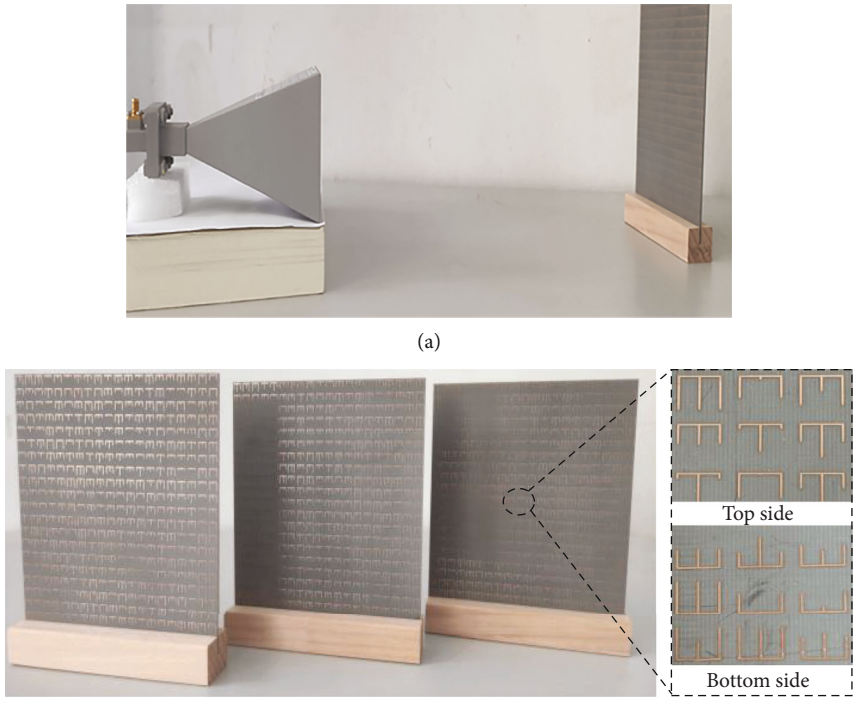

(a)

(b)

Figure 10: Transmitarray prototypes.

2.5. Advantages of This Proposed Method. Following the aforementioned design procedure, the advantages of this proposed method are summarized as follows.

(1) This method provides a novel design procedure through constructing the mapping relationship from structural parameters of TA unit cell to its transmission amplitude and phase, rather than from amplitude and phase to structural parameter. Therefore, it makes it possible to realize collaborative control of amplitude and phase through optimizing structural parameters

(2) The proposed design method has more universal applicability for TA designs, because it is not necessary to decouple transmission amplitude and phase, which is much difficult for most TA designs

(3) This optimization method extremely saves computational time because cost function is evaluated by using the predicted surrogate model, rather than expensive computer simulation and physical experiment

(4) It has fast design speed through introducing multiobjective optimization algorithm, based on the fact that all radiation performances are synthesized simultaneously and multiple structural parameters are optimized by using state-up-to-date operators without abundant parameter sweep

3. Three TA Designs

In order to verify the high efficiency of this proposed method, three TA designs with different scanning angles are designed to obtain high sidelobe suppression level. Considering its simple structure and wide phase range, a Huygens' structure is proposed to serve as a basic unit cell of these TA designs.

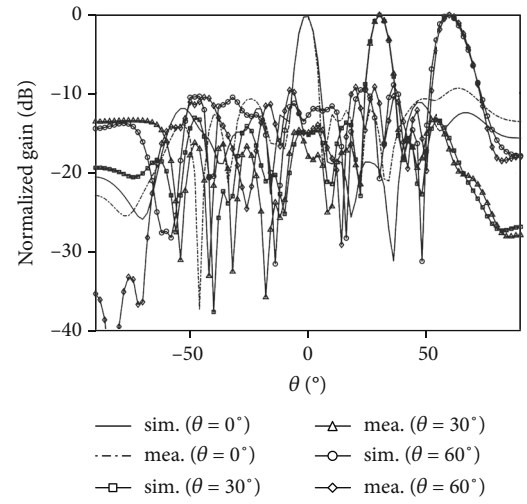

Figure 11: Simulated and measured radiation patterns at 20 GHz.

3.1. Huygens' Unit Cell. A new Huygens' structure configuration is illustrated in Figure 5. It consists of two E-shaped metal strips with the same structure dimensions and opposite directions. The two E-shaped metal strips are etched on two sides of one F4B printed circuit board. The substrate has dielectric constant of 2.2 and thickness of 1.5 mm. Compared with the Huygens' structure proposed in [2], this

Table 1: Comparisons with some state-up-to-date TA designs.

Design		Frequency (GHz)	Array scale	Layer number	Overall size (λ^3)	Amplitude control	Phase control	Amplitude and phase control	Gain (dBi)	SLL (dB)
[35]	$\theta = 0^\circ$	10	15×15	3	$5 \times 5 \times 2.75$	N	Y	—	18.9	14.3
[36]	$\theta = 0^\circ$	10	15×15	1	$7.5 \times 7.5 \times 5.37$	N	Y	—	25.4	19
[37]	$\theta = 29^\circ$	28	35×35	2	$9.7 \times 9.7 \times 5$	Y	Y	Independently	19	16.3
[38]	$\theta = 29.9^\circ$	10	13×13	1	$6.5 \times 6.5 \times 2.9$	Y	Y	Independently	N.G.	14.6
This work	$\theta = 0^\circ$	20	20×20	1	$8.6 \times 8.6 \times 3$	Y	Y	Collaboratively	25.2	19.5
	$\theta = 30^\circ$								22.6	17.4
	$\theta = 60^\circ$								20.1	11.2

N.G.: not given; Y: yes; N: no.

Table 2: Comparisons of computational time (unit: hours).

Design	NSGA-II-DE		MOEA/D-DE		Proposed MOEA/D-DE-GP	
	Mean	Std.	Mean	Std.	Mean	Std.
I	12.5	0.08	10.7	0.01	6	0.002
II	11.9	0.07	11.7	0.03	6	0.001
III	12.4	0.12	9.3	0.02	6	0.002

Std.: standard deviation.

proposed unit cell has simpler structure and less structural parameters to provide 360° phase range.

In this paper, a commercial simulation software, Ansys HFSS 2021, is utilized to simulate the transmission coefficients of the proposed unit cell with periodic boundary condition and Floquet port excitation. The incident wave is set to be polarized along x-axis and propagated along the positive z-axis. In order to illustrate its working mechanism, an evolution process of the surface current distribution at 20 GHz is illustrated in Figure 6. It is observed from Figure 6 that, at $T = 0$ and π, opposite current directions at the overlapping regions between top and bottom strips are equivalent to three magnetic dipoles. Three electric dipoles are obtained at $T = \pi/2$ and $3\pi/2$. Therefore, the proposed structure could serve as a Huygens' unit cell.

Figure 7 illustrates both transmission amplitude and phase versus structural parameters, a and b. It is observed from Figure 7 that no matter how a changes from 2.4 mm to 4.4 mm, 360° transmission phase shift could be obtained through varying b from 0 mm to 4.4 mm. Transmission amplitude varies from 0.1 to 0.95. The design space of transmission amplitude and phase is $[0.1, 0.95] \times [0^\circ, 360^\circ]$. Therefore, this structure could provide enough degree of freedom in terms of amplitude attenuation and phase shift.

3.2. Accuracy of GP-Based Surrogate Model. In this paper, two GP models are employed to predict transmission amplitude and phase, respectively. Hypercubic sampling method is used to generate 900 training data, where structural parameters a and b are sampled with equal interval. In addition, another 800 data are used as test data to verify the accuracy of the trained surrogate models.

Figure 8 lists the comparison results in terms of transmission amplitude and phase. Great agreement between fitted values and true values is observed from Figure 8. Actually, the MAEs of these two GP models are 0.036 and 0.007, respectively. The probabilities of the true values being in the prediction interval are 0.980 and 0.964, respectively.

Therefore, it could be concluded that the trained GP-based surrogate models could predict the true transmission amplitude and phase accurately.

3.3. Three TA Designs. Three TA designs with scanning angles of $\theta = 0^\circ$, 30°, and 60° (denoted as designs I, II, and III) are designed in this section. Each TA has 20×20 unit cells, and the element spacing is set as 0.43λ (λ: the free-space wavelength at 20 GHz). By using the proposed MOEA/D-DE-GP, required amplitude and phase distribution are obtained and shown in Figure 9.

All TAs are fabricated and tested in Figure 10. During measurement, a linearly polarized horn with 90° half-power beam width (HPBW) is used to feed the designed TAs, respectively, and the focal distance F is set as 3λ to ensure the whole TA could be well excited [4, 28].

Both measured and simulated radiation patterns are shown in Figure 11. From Figure 11, great agreement between simulation and measurement results is observed. Measured SLLs of these designs are lower than 19.5 dB, 17.4 dB, and 11.2 dB, respectively. It should be noticed that the measured SLL at boresight direction is 7.5 dB higher than general 12 dB. In addition, comparisons with some state-up-to-date TA designs are listed in Table 1. When scanning angle is equal to 0°, compared with [35, 36], design I in this work has a maximum SLL. When scanning angle is around 30°, compared with [37, 38], design II in this work also presents a maximum SLL. Therefore, these TAs have higher sidelobe suppression levels by using the proposed collaborative control method of transmission amplitude and phase.

In order to verify the high efficiency of this proposed method, comparisons in terms of computational time with original MOEA/D in [34] and another popular population-based computational intelligence method, NSGA-II (enhanced nondominated sorting genetic algorithm) [39], are given in Table 2. Based on the fact that all optimization algorithms are heuristic search algorithms, all of them are run for 20 times, independently. In the implementations of both original MOEA/D and NSGA-II, like [32, 33], HFSS 2021 is utilized for objective function evaluation. The computational time for each objective function evaluation conducted on a PC with Intel Core 4@3.5 GHz is 0.4 minutes. All algorithms are implemented through C/C++ and is combined with HFSS through VBScript [32, 33]. Population size is set as 50. The stop condition is set as the first time when comparable designs in Table 1 are obtained. All objective function evaluations in MOEA/D-DE and NSGA-II-DE (NSGA-II combined with differential evolution operators) are conducted through full-wave EM simulations, while the objective function evaluations in MOEA/D-DE-GP are realized by using GP-based surrogate models. It is observed from Table 2 that MOEA/D-DE-GP takes less and stable computational time, which is equal to the total EM simulation time of 900 sample points. Therefore, it is concluded that the proposed method takes less computational time and has better algorithm stability.

Therefore, it could be concluded that the proposed MOEA/D-DE-GP could provide a well collaborative control method of transmission amplitude and phase of transmitarray antenna for sidelobe suppression.

4. Conclusions

In this paper, a collaborative control method of transmission amplitude and phase is proposed for TA design. In this method, GP-based surrogate model is trained at first, and then, MOEA/D-DE-GP serves as an optimizer to obtain optimal structural parameters of TA. Three TAs with high sidelobe suppression level are designed, where accuracy of GP-based surrogate model is verified. It could be concluded from measured results that the proposed collaborative control method of amplitude and phase is much promising for high sidelobe suppression level in TA designs.

Data Availability

The source codes of GP model used to support the findings of this study are available from the corresponding author upon request after publication of this article.

Conflicts of Interest

The authors declare that they have no conflicts of interest.

Acknowledgments

This work was supported in part by the Key Research and Development Program of Anhui Province under Grant 2022a05020045.

References

[1] X.-H. Jiao and G. Wan, "A novel low-profile planar microstrip transmitarray antenna with high efficiency," *International Journal of RF and Microwave Computer-Aided Engineering*, vol. 31, no. 5, Article ID e22614, 2021.

[2] C. Xue, Q. Lou, and Z. Chen, "Broadband double-layered Huygens' metasurface lens antenna for 5G millimeter-wave systems," *IEEE Transactions on Antennas and Propagation*, vol. 68, no. 3, pp. 1468–1476, 2020.

[3] Y. Shi, Q. Zeng, Z. Xue, W. Ren, and W. Li, "Dual-band double circularly polarized wide-angle beam-scanning antenna using planar phase gradient transmitarrays," *International Journal of RF and Microwave Computer-Aided Engineering*, vol. 32, no. 7, Article ID e23170, 2022.

[4] H. Li, G. Wang, T. Cai, H. Hou, and W. Guo, "Wideband transparent beam-forming metadevice with amplitude-and phase-controlled metasurface," *Physical Review Applied*, vol. 11, no. 1, article 014043, 2019.

[5] J. Ding, N. Xu, H. Ren, Y. Lin, W. Zhang, and H. Zhang, "Dual-wavelength terahertz metasurfaces with independent phase and amplitude control at each wavelength," *Scientific Reports*, vol. 6, no. 1, pp. 1–9, 2016.

[6] H. Li, G. Wang, T. Cai, J. Liang, and X. Gao, "Phase-and amplitude-control metasurfaces for antenna main-lobe and sidelobe manipulations," *IEEE Transactions on Antennas and Propagation*, vol. 66, no. 10, pp. 5121–5129, 2018.

[7] H. Xu, G. Hu, L. Han et al., "Chirality-assisted high-efficiency metasurfaces with independent control of phase, amplitude, and polarization," *Advanced Optical Materials*, vol. 7, no. 4, article 1801479, 2019.

[8] J. Abras, T. Tuckey, D. McDaniel, and N. Hariharan, "Adaptive training investigation to support machine learning based surrogate modeling for aircraft loads predictions," in *AIAA SCITECH 2024 Forum*, p. 1942, Orlando, FL, 2024.

[9] J. Du, H. Cao, Y. Li, Z. Yang, A. Eslamimanesh, and M. Fakhroleslam, "Development of hybrid surrogate model structures for design and optimization of CO2 capture processes: part I. Vacuum pressure swing adsorption in a confined space," *Chemical Engineering Science*, vol. 283, article 119379, 2024.

[10] O. Piltan, A. Kizilay, M. Belen, and P. Mahouti, "Data driven surrogate modeling of horn antennas for optimal determination of radiation pattern and size using deep learning," *Microwave and Optical Technology Letters*, vol. 66, no. 1, article e33702, 2024.

[11] H. Li, Y. Wang, J. Zhu, and M. Han, "Performance map and operating condition optimization of industrial-size SOFCs using a PINN surrogate model," *International Journal of Hydrogen Energy*, vol. 50, pp. 1294–1307, 2024.

[12] J. Donnelly, A. Daneshkhah, and S. Abolfathi, "Physics-informed neural networks as surrogate models of hydrodynamic simulators," *Science of the Total Environment*, vol. 912, article 168814, 2024.

[13] A. Pietrenko-Dabrowska and S. Koziel, "Fast EM-driven parameter tuning of microwave circuits with sparse sensitivity updates via principal directions," *Knowledge-Based Systems*, vol. 252, article 109388, 2022.

[14] S. Koziel, A. Pietrenko-Dabrowska, and U. Ullah, "Tolerance-aware optimization of microwave circuits by means of principal directions and domain-restricted metamodels," *IEEE*

Transactions on Microwave Theory and Techniques, vol. 70, no. 9, pp. 4085–4093, 2022.

[15] P. Mahouti, M. Belen, N. Çalık, and S. Koziel, "Computationally efficient surrogate-assisted design of pyramidal-shaped 3D reflectarray antennas," *IEEE Transactions on Antennas and Propagation*, vol. 70, no. 11, pp. 10777–10786, 2022.

[16] P. Mahouti, F. Güneş, M. A. Belen, and S. Demirel, "Symbolic regression for derivation of an accurate analytical formulation using "big data" an application example," *Applied Computational Electromagnetics Society Journal*, vol. 32, no. 5, pp. 372–380, 2017.

[17] A. Kayabasi, A. Toktas, A. Akdagli, M. Bicer, and D. Ustun, "Applications of ANN and ANFIS to predict the resonant frequency of l-shaped compact microstrip antennas," *Applied Computational Electromagnetics Society Journal*, vol. 29, no. 6, pp. 460–469, 2014.

[18] D. Klink and M. Petrie, "A comparison of techniques for finding coefficients of polynomial chaos models for antenna problems," *International Journal of RF and Microwave Computer-Aided Engineering*, vol. 31, no. 8, Article ID e22729, 2021.

[19] A. Belen, O. Tari, P. Mahouti, M. Belen, and A. Çalışkan, "Surrogate-based design optimization of multi-band antenna," *Applied Computational Electromagnetics Society Journal*, vol. 37, no. 1, pp. 34–40, 2022.

[20] P. Ashish and S. Gupta, "Optimization of ultra-wide band antenna by selection of substrate material using artificial neural network," *Applied Physics A*, vol. 128, no. 3, p. 192, 2022.

[21] T. Khan and C. Roy, "Prediction of slot-position and slot-size of a microstrip antenna using support vector regression," *International Journal of RF and Microwave Computer-Aided Engineering*, vol. 29, no. 3, Article ID e21623, 2019.

[22] S. Longobardi, A. Lewalle, S. Coveney et al., "Predicting left ventricular contractile function via Gaussian process emulation in aortic-banded rats," *Philosophical Transactions of the Royal Society A*, vol. 378, no. 2173, article 20190334, 2020.

[23] C. Rasmussen and C. Williams, *Gaussian Processes for Machine Learning*, MIT Press, Cambridge, MA, 2015.

[24] Q. Zhang, W. Liu, W. Tsang, and B. Virginas, "Expensive multiobjective optimization by MOEA/D with Gaussian process model," *IEEE Transactions on Evolutionary Computation*, vol. 14, no. 3, pp. 456–474, 2010.

[25] Q. Zhang and H. Li, "MOEA/D: a multiobjective evolutionary algorithm based on decomposition," *IEEE Transactions on Evolutionary Computation*, vol. 11, no. 6, pp. 712–731, 2007.

[26] C. Nurullah, F. Güneş, S. Koziel, A. Pietrenko-Dabrowska, A. Mehmet, and P. Mahouti, "Deep-learning-based precise characterization of microwave transistors using fully-automated regression surrogates," *Scientific Reports*, vol. 13, no. 1, p. 1445, 2023.

[27] S. Simon, G. Schwarz, A. Aichmair et al., "Fully automated deep learning for knee alignment assessment in lower extremity radiographs: a cross-sectional diagnostic study," *Skeletal Radiology*, vol. 51, no. 6, pp. 1249–1259, 2022.

[28] A. Clemente, L. Dussopt, R. Sauleau, P. Potier, and P. Pouliguen, "Wideband 400-element electronically reconfigurable transmitarray in X band," *IEEE Transactions on Antennas and Propagation*, vol. 61, no. 10, pp. 5017–5027, 2013.

[29] R. Mailloux, *Phased Array Antenna Handbook (2nd Version)*, Artech House, Norwood, MA, USA, 2005.

[30] D. Ding, J. Xia, L. Yang, and X. Ding, "Multiobjective optimization design for electrically large coverage: fragment-type near-field/far-field UHF RFID reader antenna design," *IEEE Antennas and Propagation Magazine*, vol. 60, no. 1, pp. 27–37, 2018.

[31] D. Ding, Q. Zhang, J. Xia, A. Zhou, and L. Yang, "Wiggly parallel-coupled line design by using multiobjective evolutionay algorithm," *IEEE Microwave and Wireless Components Letters*, vol. 28, no. 8, pp. 648–650, 2018.

[32] D. Ding, X. Ding, S. Ling, and H. Zhang, "A novel computational intelligence method for broadband dual-polarized base station antenna design," *International Journal of RF and Microwave Computer-Aided Engineering*, vol. 32, no. 1, Article ID e22946, 2022.

[33] D. Ding, X. Ding, H. Zhang, and S. Ling, "Locating Pareto optimal designs of antenna through parallel multiobjective evolutionary algorithm," *International Journal of RF and Microwave Computer-Aided Engineering*, vol. 31, no. 11, Article ID e22871, 2021.

[34] H. Li and Q. Zhang, "Multiobjective optimization problems with complicated Pareto sets, MOEA/D and NSGA-II," *IEEE Transactions on Evolutionary Computation*, vol. 13, no. 2, pp. 284–302, 2009.

[35] B. Liu and C. Song, "High gain transmitarray antenna based on ultra-thin metasurface," *International Journal of RF and Microwave Computer-Aided Engineering*, vol. 29, no. 5, Article ID e21655, 2019.

[36] H. Zhu, L. Guo, and W. Feng, "A low-profile transmitarray antenna using square patch elements with cross dipole slots and vias," *International Journal of RF and Microwave Computer-Aided Engineering*, vol. 30, no. 4, Article ID e22106, 2020.

[37] Q. Lou and Z. Chen, "Sidelobe suppression of metalens antenna by amplitude and phase controllable metasurfaces," *IEEE Transactions on Antennas and Propagation*, vol. 69, no. 10, pp. 6977–6981, 2021.

[38] Y. Yuan, C. Huang, J. Ding, and C. Guo, "A low-profile low-sidelobe beam steering metasurface lens based on amplitude-phase control," *Microwave and Optical Technology Letters*, vol. 65, no. 8, pp. 2150–2157, 2023.

[39] K. Deb, A. Pratap, S. Agarwal, and T. Meyarivan, "A fast and elitist multiobjective genetic algorithm: NSGA-II," *IEEE Transactions on Evolutionary Computation*, vol. 6, no. 2, pp. 182–197, 2002.